Journal of Ubiquitous Systems & Pervasive Networks
Volume 5, No. 1 (2014) pp. 09-16

Electromagnetic Energy and Data Transfer for a Neural Implant

Navid Rezaei[a] *, Deyasini Majumdar[b], Bruce Cockburn[a], Christian Schlegel[b]

[a]*Department of Electrical and Computer Engineering, University of Alberta, Edmonton, Canada, T6G 2V4*
[b]*Department of Electrical and Computer Engineering, Dalhousie University, Halifax, Canada, B3H 4R2*

Abstract

The wireless transfer of energy through living tissues for the purpose of data communications is investigated. After considering the best frequency band for communications in biological tissues, both the uplink and downlink near-field coupled energy transfer options are analyzed. The possibility of wireless powering using the same frequency band is also studied. The nominal power consumption of the implantable baseband communications circuitry was estimated for smaller technology nodes using the Synopsys CAD tools. The effect of using the ultra low power subthreshold operation in different technology nodes was also analyzed using predictive technology models. By introducing an analysis flow and the corresponding implementation code, we were also able to predict the subthreshold power consumption of the circuitry in different technology nodes and importantly at the gate level.

Keywords: near-field, link budget, implant, wireless communications, ultra-low power, subthreshold

1. Introduction

Implantable biomedical systems will play an important role in the future of medical systems. Some successful implants have already been used for years, such as cardiac pacemakers. Implants usually need to transmit out sensory information and also receive power and command signals from outside of body.

In order for an implant to communicate with an external control system, either transmitting or receiving, different communications methods have been considered. One approach is to use a wired connection between the implant and the external device, as in [1, 2]. A wired connection through the skin however, presents a channel for infections and is not viable for long-term use. Another method is to use an optical connection, such as the vertical-cavity surface-emitting laser (VCSEL), as in [3]. Although we can achieve very high-data rates using an optical connection, communications is limited to very short distances and is dependent on precise alignment of the transmitter and receiver. Therefore, an optical connection can be used only for applications where the transmitter and receiver can be kept close and stationary. Another option is to use radio-frequency (RF) transmission. However, electrical antennas typically used for RF transmission experience a shift in the resonance frequency unless a sufficiently thick dielectric insulation is used [4]. Thick dielectric insulation reduces the form factor advantage of small electric antennas, such as patch antennas, compared to high-frequency loop antennas, which can be designed much smaller, even 100-fold, than conventional low-frequency coils, without sacrificing efficiency [5]. We analyze near-field RF transmission as a method for communicating with an implant since it can accommodate several centimeters of implantation depth, uses coils that are not significantly detuned by surrounding tissues, and is advantageous in a noisy environment, as discussed later. Although our specific purpose is to transmit high data rate spinal neural recording data (order of Mbps), the results can be applied to other implant scenarios. This paper is organized as follows: Section 2 considers tissue characteristics and its effects on frequency and antenna selection. Section 3 analyzes the near-field coupled uplink for data transfer. Section 4 discusses the feasibility of downlink communications and power transfer. Section 5 discusses about the circuitry's power consumption. Concluding remarks are made in Section 6.

2. Tissue Characteristics and its Effects on Frequency and Antenna Selection

Body tissue characteristics must be considered with utmost care since the presence of tissue in the transmission path can have effects on the tuning of the antennas, the optimal

* Corresponding author.
E-mail: nrezaeis@ualberta.ca

DOI: 10.5383/JUSPN.05.01.002

frequency for energy transfer and the capacity of the channel as the loss is increased.

To better analyze the effects of tissue over a broad spectrum of frequencies, we need a model that can provide accurate predictions at different frequencies. Two models for biological tissues are the Cole-Cole and Debye models, which are variants of each other [6]. The Debye model can be written as [7, 8]:

$$\epsilon_r(\omega) = \epsilon_\infty + \frac{\epsilon_{r0} - \epsilon_\infty}{1 - j\omega\tau} + j\frac{\sigma}{\omega\epsilon_0} \quad (1)$$

where τ is the relaxation time constant, ω is the angular frequency under investigation, ϵ_∞ is the relative permittivity at high frequencies where $\omega \gg 1/\tau$, ϵ_{r0} is the static relative permittivity, ϵ_0 is the permittivity of vacuum, and σ is the conductivity of the tissue.

The wavenumber k, which is defined using $k^2 = \omega^2\mu\epsilon$, can be approximated by

$$k \approx \omega\sqrt{\mu_0\epsilon_0\epsilon_{r0}} + j\frac{\omega}{2}\sqrt{\frac{\mu_0\epsilon_0}{\epsilon_{r0}}}\left(\frac{\sigma}{\omega\epsilon_0} + \omega\tau\Delta\epsilon\right) \quad (2)$$

To quantitatively analyze the amount of power absorbed by biological tissue, we can use the absorption coefficient defined in [9] as $\alpha = 2\kappa$, where κ is the imaginary part of the wavenumber ($\kappa = \mathrm{Im}(k)$). Using this definition, the absorption coefficient is calculated as

$$\alpha = (\sigma + \omega^2\tau\epsilon_0\Delta\epsilon)\sqrt{\frac{\mu_0}{\epsilon_0\epsilon_{r0}}} \quad (3)$$

Over a large range, the absorption coefficient is constant with frequency for $\omega \ll \sqrt{\sigma/\tau\epsilon_0\Delta\epsilon}$ (lower frequency) and then grows with the square of ω when $\omega \gg \sqrt{\sigma/\tau\epsilon_0\Delta\epsilon}$ (higher frequency).

As the tissue absorption increases with frequency, it is often assumed lower frequencies, in order of MHz, result in better transfer efficiency. Omitting the displacement current ($j\omega\epsilon\vec{E}$) in Maxwell's equations due to low frequency leads to the result that the length of diffusion becomes inversely proportional to square of frequency and this confirms that higher frequencies decay faster in tissue. However, the mentioned diffusion approximation is valid for good conductors and tissue is better modeled as a low-loss dielectric with significant displacement current. Solving the Helmholtz equation shows that the penetration depth is asymptotically independent of frequency. On the other hand, the received power is proportional to frequency of the incident magnetic field and this suggests that higher frequency results in higher efficiency. As discussed earlier, the Debye model for tissue leads to higher absorption coefficients at higher frequencies, which leads to a possible optimal frequency for energy transfer [8]. According to the calculations in [8], the optimal electromagnetic energy transfer frequencies in skin (wet), fat (infiltrated), muscle and blood with 1 cm implant depth are 4.01 GHz, 6 GHz, 3.93 GHz and 3.54 GHz, respectively.

Knowing the optimal frequency to be in the low-GHz range [8], we need to consider the best-licensed band to use. The licensed Medical Implant Communications Service (MICS) band is around 400 MHz, which is far below the optimal frequency range. Among the ISM bands, the 5.8-GHz band does not have good penetration into biological tissues [10]. Although the 900-MHz ISM band is close to the low-GHz range, its bandwidth is less than the 2.4-GHz ISM band and is not as widely accepted worldwide as the 2.4-GHz ISM band. Based on the frequency optimality, the amount of available bandwidth and its worldwide acceptance as a licensed band, we chose the 2.4-GHz ISM band in our work.

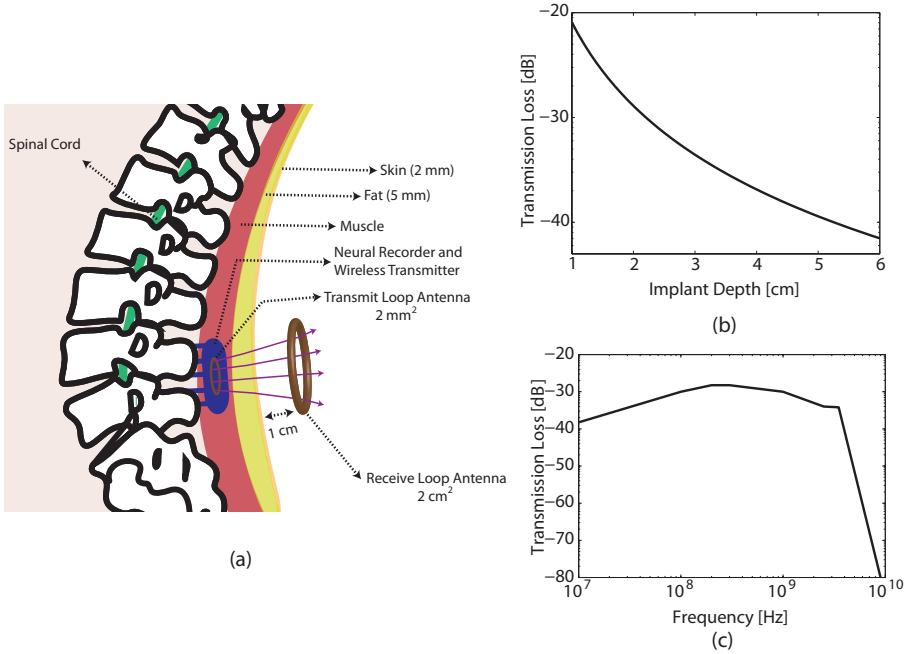

Fig. 1. Coupled energy transfer characteristics: (a) location of the transmitter close to the spinal cord and the receiver above the skin (b) the associated optimal path loss for the optimal frequency [8] (c) Simulated path loss with conjugate matching at receiver with square transmitter and implant depth of 2 cm [8].

3. Near-field Uplink Budget Analysis

If the antennas are linear and bidirectional; and the heterogeneous medium is linear and isotropic, we can conclude that the transfer efficiency is the same along the uplink and downlink paths. According to Fig. 1.b, reproduced from [8], the amount of path loss at the center frequency of the 2.4-GHz ISM band is roughly -30 dB. Using different antenna designs may affect the optimal frequency, but transfer efficiencies of around the same value are still achievable as shown in [11] for 115 MHz.

3.1. Noise in the 2.4-GHz ISM band

To calculate the amount of the received signal-to-noise ratio (SNR), it is important to model the noise correctly. In this part, we consider the noise power spectral density (PSD) at the receiver for coupled uplink communications from an implant to an external receiver over the 2.4-GHz ISM band.

The noise power spectral density (PSD) in the 2.4-GHz ISM band is not the usual thermal noise since it includes signals from man-made WiFi and Bluetooth systems. Experimental measurements of noise levels in the 2.4-GHz ISM band are reported in [12]. The temperature at which the measurements were made was $T_0 = 296$ K, which leads to a thermal noise power spectral density of -114 dBm/MHz. Averaging the values from the two urban site measurements (both horizontal and vertical) leads to an average noise PSD of -86 dBm/MHz. The receiver used has a 3-dB noise figure. By subtracting the noise figure, we end up with an average -89 dBm/MHz noise PSD in the 2.4-GHz ISM band at 296 K. Therefore, we can conclude that man-made sources exceed the thermal noise floor by roughly 25 dB.

In biomedical applications, since the receiver antenna is facing the body, the ambient temperature is 37 ° C (310.15 K). This leads to an approximate thermal noise power spectral density of -113.5 dBm/MHz, which still leads to a number close to -89 dBm/MHz if one includes 25 dB from man-made sources.

The man-made signals mostly originate from sources for which the receive antenna is in the far field. A loop antenna has a low radiation resistance, which reduces the effective area and therefore the received far-field man-made signal power. An antenna's effective area is the ratio of the available power at the terminals of a receiver antenna to the incident plane-wave's power flux density. The amount of received noise depends on the antenna's maximum effective area, which is calculated as follows (assuming a small single-turn circular receive loop and plane-wave man-made signals) [9]

$$A_{em} = \left(\frac{R_r}{R_r + R_L} \right) \cdot \left(\frac{3\lambda^2}{8\pi} \right) \qquad (4)$$

where $R_r = 20\pi^2 (C/\lambda)^4$ is the radiation resistance, $R_L = (C/2\pi b)\sqrt{\omega\mu_0/2\sigma}$ is the loss resistance, C is the loop's circumference, b is the wire radius, and σ is the wire conductivity. We have assumed no reflection loss and no polarization mismatch. In the antenna's equivalent circuit, the radiation resistance (R_r) is the equivalent resistance accounting for the amount of radiation and the loss resistance (R_L) is the equivalent resistance accounting for the ohmic antenna losses.

Even assuming no reflection loss and no polarization mismatch leads to -27.65 dB maximum effective area for the receiver loop antenna with area of 2 cm^2 and 0.5- mm wire radius. This means that man-made noise is not a dominant noise source for a typical loop antenna and the noise level is roughly equal to the thermal noise level.

3.2. Quality of Reception

The quality of reception using spread spectrum modulated packet transmission is determined by two probabilities: one is the probability of missing a packet and the second is the probability of having a false alarm [13]. To have a reasonable amount of reception quality, $P(miss)$ and $P(false)$ are considered to be 10^{-6} and 10^{-3}, respectively. According to [13], the signal-to-noise ratio (SNR) for the packet preamble is defined as $\text{SNR}_\text{p} = PL_bE_c/N_0$, where L_b is the processing gain, P is the preamble length, and E_c/N_0 is the energy of each chip over the noise power spectral density. Using Fig. 3 in the paper, the values of $P = 10$ and $L_b = 5$ were used, together with the assumptions that $P(miss) = 10^{-6}$ and $P(false) = 10^{-3}$, and hence the required SNR_p should roughly be 17 dB for the preamble. Based on the definition of the preamble SNR, the E_c/N_o value should be equal to 0 dB.

3.3. Link Budget

As explained in Sec. 3.2, to achieve minimum reception quality, the required E_c/N_o has to be no less than 0 dB. With $L_b = 16$, we have: $E_b/N_o = L_b \cdot E_c/N_o = 12$ dB. The received SNR is given by [14]

$$SNR = 10\log\left(\frac{E_c}{N_0} \cdot \frac{R_c}{W_n} \right) \text{ [dB]} \qquad (5)$$

where R_c is the chip rate in chips per second and W_n is the noise bandwidth in Hz.

Based on the link budget calculations in Appendix A, the energy to transmit one bit is computed as

$$E_{bt} \approx kT_0 \cdot \frac{E_b}{N_0} \cdot 10^{\left((NF - P_L)/10\right)} \text{ [J/bit]} \qquad (6)$$

The uplink budget is detailed in Table 1. To calculate the required transmit power for a specific data rate, we multiply the transmission energy per bit (in this case ~68 pJ/bit) by the data rate. For example, to achieve a data rate of 2 Mbps, the required transmit power is equal to ~ 68 pJ/bit $\times 2$ Mbps ≈ 136 μW or -8.6 dBm.

4. Near-field Downlink Budget Analysis

The downlink can be used for both powering the implant and data communications. Since the path loss is the

same for the up- and downlink [8] and given that the man-made signals are attenuated in human tissue but still keeping the margin, we can use the same link budget as the uplink. We conclude that around 68 pJ/bit is required to transmit one bit in the downlink using the spread spectrum modulation scheme.

It has been shown in [8] that up to 1 mW of power could be transferred to a mm-sized receive antenna by a cm-size transmit antenna within a few cm of separation. This amount is enough to power a low-power implant for continuous real-time operation. In our case, we are expecting a few milliwatts of power including the neural recording, as well as baseband and RF communications. This may necessitate a rechargeable battery or another powering scheme, such as ultrasound, for real-time powering.

Table 1. Link Budget Values to Achieve P(miss) = 10^{-6} and P(false) = 10^{-3} using Spread Spectrum Modulation in the 2.4-GHz ISM Band.

Parameters	Value
Required Quality of Reception	$P(miss) = 10^{-6}$ & $P(false) = 10^{-3}$
Required E_b/N_o	12 dB
Receiver Noise Figure	10 dB
Thermal Noise	-174 dBm/Hz
Extra Man-Made Noise Margin	-25 dB
Path Loss (2 cm tissue depth)	-30 dB
Fading Margin	-10 dB
Excess Loss	-15 dB
Energy Required to Transmit a Bit	68 pJ/bit
Approximate Required Transmit Power (Assuming data rate of 2 Mbps)	-8.6 dBm

5. Circuitry Power Consumption

It has been shown in [8] that up to 1 mW of power could be transferred to a mm-sized receive antenna by a cm-size transmit antenna within a few cm of separation. This amount is enough to power a low-power implant for continuous real-time operation. We therefore need to know how much power is consumed by a typical implantable high data rate transmitter system using spread spectrum modulation in the 2.4-GHz ISM band. As shown in Fig. 1, an RF wireless transmitter for implant purposes, such as neural recording, consists of baseband communications subsystem and RF front-end.

5.1. Nominal Voltage

The original version of the baseband transmitter IC in the group is developed in 130 nm IBM technology [15]. Operated in 1.2 V nominal supply voltage and 12.5 MHz chip clock frequency, the chip includes baseband transmitter, testing units and pulse shaping filter. The power consumption is 600 μW and thus the associated energy consumption efficiency is 768 pJ/bit at 12.5 MHz chip clock frequency. Using smaller technology nodes, removing testing units and shaping filter and also operating the circuitry in subthreshold regime can further reduce the power consumption of the spread-spectrum-based baseband design.

Scaling down to 65-nm technology has promised power reduction [16]. However, smaller than 65 nm technology nodes suffer from more leakage currents, which increases the static power consumption compared to bigger technology nodes. The issue needs further research to mitigate the problem. Using the Synopsys Design Compiler tool, we analyzed the amount of possible power reduction due to using TSMC's 65-nm technology at a 1 V nominal supply voltage at the same data rate as in the IBM 130-nm case (3.125 Mbps). The total baseband power consumption in 65-nm TSMC process by removing the JTAG test mode units and the shaping filter is expected to be roughly 370 μW (118 pJ/bit at 3.125 Mbps). The power consumption can be even further reduced by operating in the subthreshold regime, which is suitable for medium throughputs (1-10 MHz) [16]. In subthreshold operation, the transistors are either kept off (non-conducting) or just short of conducting in the triode region (barely conducting). The relatively high on resistance of the barely conducting transistors will slow down the operation of logic gates and storage elements.

Assuming 4.5 mW of expected power consumption for the RF front end at TSMC's 65-nm technology and 370 μW for the baseband circuitry in TSMC's 65-nm process, the resulting transmitter circuit power consumption is 4.87 mW (1.56 nJ/bit at 3.125 Mbps). Note that the baseband power consumption for spread spectrum modulation is much less than the required power consumption for the RF front-end circuitry, which is in the order of milliwatts. As calculated in Sec. 3, the energy required to transmit one bit from the transmit antenna to the receive antenna is ~68 pJ/bit. Therefore the energy absorbed by the path loss is negligible compared to the energy required to drive the transmitter circuitry. Based on these numbers, the overall power consumption is expected to be above one milliwatt, which is the maximum wireless power that could be delivered safely to the implant [8]. This may necessitate a rechargeable battery or another powering scheme, such as ultrasound, for real-time powering.

5.2. Subthreshold Regime

To further reduce the power consumption of the baseband transmitter, we can use the subthreshold regime for medium throughputs. It has been shown in [17] (Chapter 1) that we can save almost up to a factor of 15 in energy per operation by using a 0.3 V subthreshold supply voltage in place of the 1.3 V nominal voltage in 130 nm CMOS. To study the effects of technology scaling on the power consumption of subthreshold circuits, we have done a trend analysis on baseband circuit power consumption in subthreshold through different technology nodes. This analysis is based on a

theoretical gate-level reconstruction of the baseband transmitter and is not intended to reach exact numbers. However, it should clarify the approximate trends on how power consumption may be reduced by using smaller technology nodes in the subthreshold regime.

To calculate the power consumption of each logic gate, we consider the output switching capacitance of the logic gate to calculate the dynamic power consumption and the leakage current for the static power consumption. By having the power consumption for each logic gate, we can proceed to the next level and calculate the power consumption of each cell. By cell, we mean the main building blocks of the circuit, which are shift registers, flip-flops, multiplexers, and some logic gates.

To calculate the power consumption in the subthreshold regime, we have assumed the bit frequency f_1 to be sixteen times smaller than the chip frequency f_2 ($f_1 = f_2/16$). Loading capacitances for gates are approximated to be equal to the FO4 inverter capacitive or in some cases more or less than the FO4 inverter capacitance loadings based on the gate location. Although it is not always in the subthreshold regime, we consider the V_{dd} to be in the range of 0.2 V to 0.5 V. The threshold voltages of the 32 nm, 45 nm, 65 nm, 90 nm, 130 nm, 180 nm and 250 nm technologies are 0.27 V, 0.27 V, 0.3 V, 0.32 V, 0.36 V, 0.49 V and 0.63 V, respectively. We also assume that the switching factor of 0.5 represents an upper bound. The transistor data in subthreshold supply voltages is used from the data of [16]. The energy consumption of the circuit in different technologies and subthreshold supply voltages is demonstrated in Fig. 2. As it is demonstrated in this figure, in smaller technologies the effect of subthreshold current cannot be neglected. In smaller supply voltages the increased static energy consumption increases the total energy consumption per operation. This trend leads to a sweet spot in terms of the optimal supply voltage. For example, in case of using 65 nm technology the optimal voltage for subthreshold energy consumption is between 0.2 V and 0.3 V.

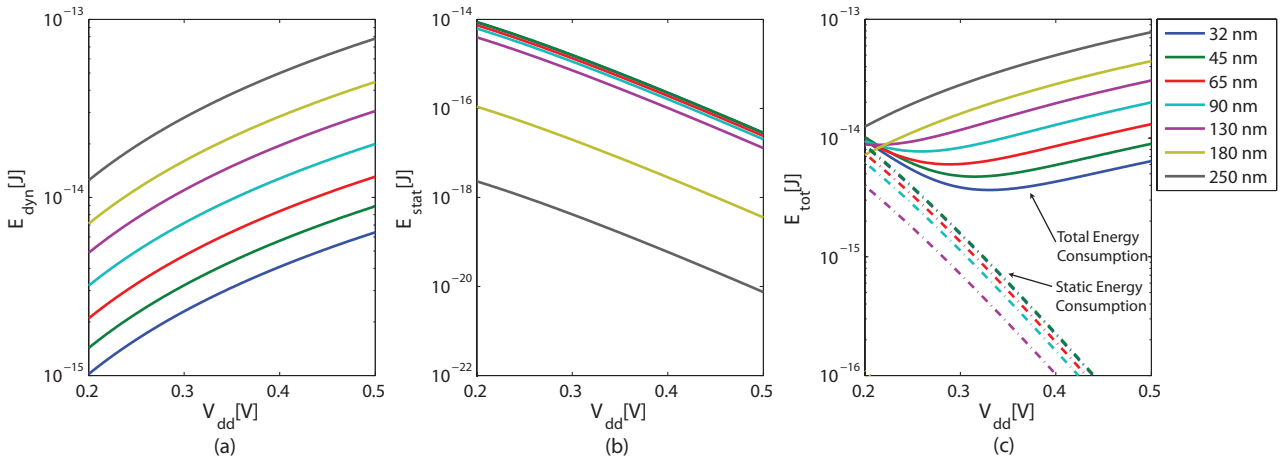

Fig. 2. Energy consumption of the baseband transmitter circuit assuming capacitive loading: (a) Dynamic energy consumption (b) Static energy consumption (c) Total energy consumption is plotted in solid line style and static energy consumption is plotted in the same figure in dotted line style.

To further verify our results, we can compare the calculated energy consumptions with multiplier energy consumption calculated in [16]. As the calibration curves in Fig. 3 show for the 65-nm technology our calculated numbers are approximately linearly aligned by the results in [16].

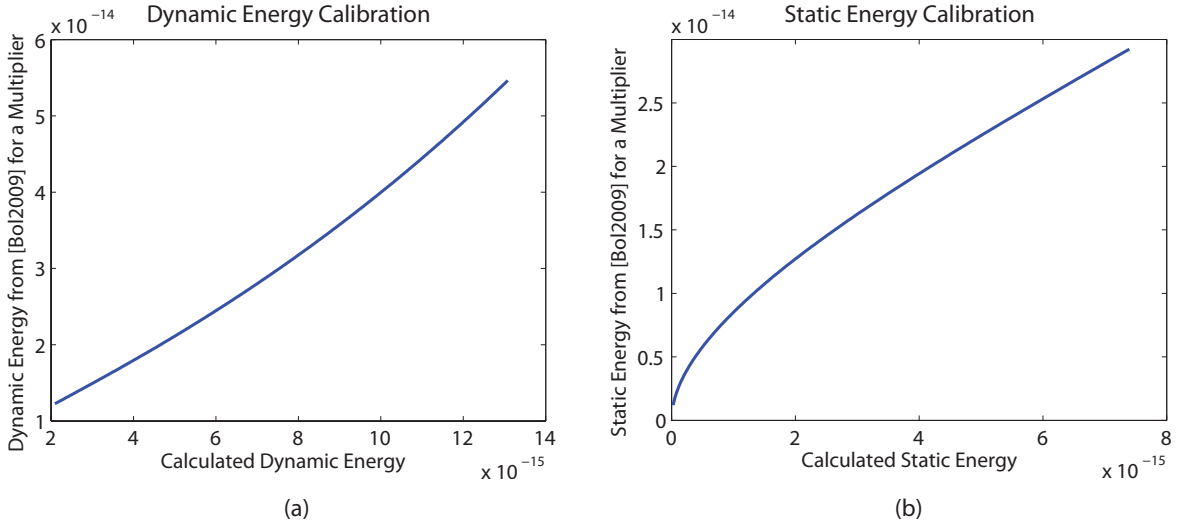

Fig. 3. Calibration curves for the calculated energy results: (a) Dynamic energy consumption (b) Static energy consumption.

In Fig. 4 the total power consumption of the baseband transmitter is plotted assuming that $f_2 = 5$ MHz and $V_{dd} = 0.5$ V. If we operate at this frequency, the static power consumption becomes more significant at smaller technology nodes. This relative increase in the static power consumption increases the total power a bit in 45-nm technology. Working at $f_2 = 5$ MHz and with the present assumptions to calculate the final power, we determine that using smaller technologies, such as 32 nm, does not necessarily benefit us much in terms of power consumption. The low-power sweet spot thus seems to be 65-nm technology given the present knowledge and expertise. To make smaller technologies more feasible, it is necessary to invent and utilize methods to reduce the subthreshold current and therefore the overall static power consumption [18].

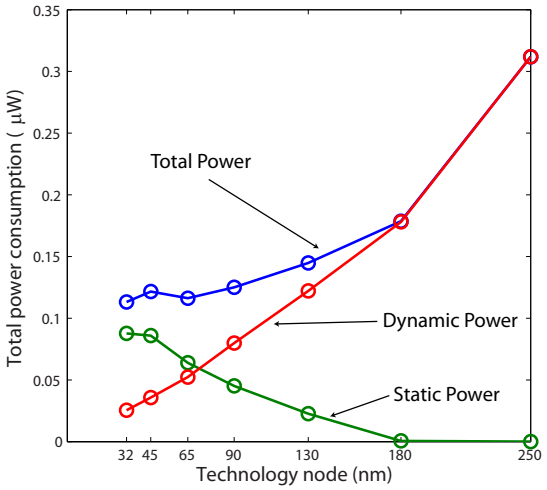

Fig. 4. Power consumption of the baseband transmitter circuit in $V_{dd} = 0.5$ V with approximated capacitive loading for each logic gate and $f_2 = 5$ MHz.

6. Conclusion

In this paper, we investigated the problem of constructing a link budget for loop antennas that are capable of wireless data transmission to devices that are implanted in biological tissues. We focused primarily on a near-field communications scenario. From several different perspectives, near-field communications is preferred over far-field communications because of lower path loss and because of greater compatibility with surrounding biological tissues. To transmit one bit on the near-field uplink or downlink in the recommended 2.4-GHz ISM band, ~68 pJ/bit of energy is required using spread spectrum modulation, when one considers the predicted link losses and gains.

The power consumption of the implanted baseband communications circuitry was estimated for TSMC's 65-nm technology using the Synopsys Design Compiler tool and the results were compared to previous results in IBM's 130-nm technology. The effect of using the ultra low-power subthreshold operation in different technology nodes was also analyzed using a generic design for the baseband transmitter. We observed that the dominant power consumption in a typical high data rate spread-spectrum implantable transmitter is due to the RF front end. According to the analysis, the transmitter circuitry cannot be safely powered in continuous operation using the described inductive links [8], as the required operation power would exceed SAR-safe inductive power transfer limits. This may necessitate a rechargeable battery to boost the power that would be provided by wireless power transfer.

The expected power consumption of the RF front end at TSMC's 65-nm technology is approximately 4.5 mW. Assuming 3.125 Mbps of data rate, the RF front end's energy consumption per bit is 1.44 nJ/bit. The expected power consumption of the baseband section at TSMC's 65-nm technology and nominal voltage is 370 μW (~118 pJ/bit at 3.125 Mbps). According to our calculations the link losses are predicted to be 68 pJ/bit. Using these numbers we plotted in Fig. 5, a pie chart that compares the energy requirements of the different modules. As we can see, the most energy is consumed in the RF front-end module. Therefore, in order to reduce the overall energy consumption drastically, more research has to be done to reduce the energy consumption in the RF front end. Data compression strategies, low bit-rate partial sleep modes and dynamic control of the RF front end should all be considered.

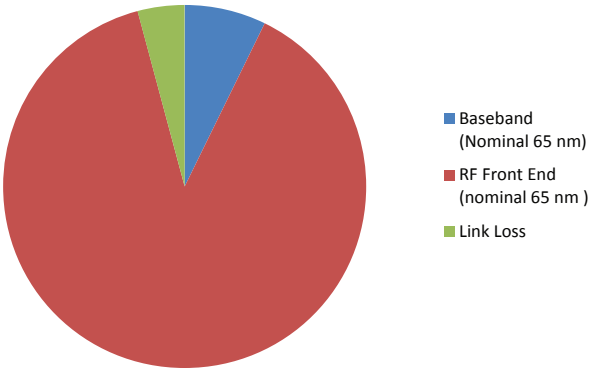

Fig. 5. Comparison of energy consumption in different modules of an implantable transmitter

As for future work, one can expand the near-field and far-field link budget results by finite-difference time-domain (FDTD) simulations in order to better understand more realistic scenarios. Concerning power consumption in the subthreshold regime, we could further take into account the limitations on the minimum supply voltage and the highest data rate possible based on industrial fabrication technologies available. For example, the minimum possible supply voltage for operation of transistors in each technology node should be calculated. There are also different process purposes in each technology, which needs to be taken care of with more details. For example, TSMC's 65-nm process has different options including General Purpose (GP) and Low Power (LP). Subthreshold operation might be preferable in the GP or LP process, but it is unclear which one should be selected.

Acknowledgement

The authors would like to thank Alberta Innovates for Health Solutions (AIHS) and the Project SMART group for their continued support, both financially and academically.

References

[1] L. Hochberg, M. Serruya, G. Friehs, J. Mukand, M. Saleh, A. Caplan, A. Branner, D. Chen, R. Penn, J. Donoghue, Neuronal ensemble control of prosthetic devices by a human with tetraplegia, Nature 442 (7099) (2006) 164–171. http://dx.doi.org/10.1038/nature04970

[2] H. Miranda, V. Gilja, C. Chestek, K. Shenoy, T. Meng, HermesD: A high-rate long-range wireless transmission system for simultaneous multichannel neural recording applications, IEEE Trans. Biomed. Circuits Syst. 4 (3) (2010) 181–191. http://dx.doi.org/10.1109/TBCAS.2010.2044573

[3] Y.-K. Song, D. Borton, S. Park, W. Patterson, C. Bull, F. Laiwalla, J. Mislow, J. Simeral, J. Donoghue, A. Nurmikko, Active microelectronic neurosensor arrays for implantable brain communication interfaces, IEEE Trans. Neural Syst. Rehabil. Eng. 17 (4) (2009) 339–345. http://dx.doi.org/10.1109/TNSRE.2009.2024310

[4] A. J. Johansson, Wireless communication with medical implants: Antennas and propagation, Ph.D. thesis, Lund University (2004).

[5] A. Poon, Miniaturization of implantable wireless power receiver, in: Engineering in Medicine and Biology Society (EMBC). Annual International Conference of the, IEEE, 2009, pp. 3217–3220.

[6] S. Gabriel, R. Lau, C. Gabriel, The dielectric properties of biological tissues: III. Parametric models for the dielectric spectrum of tissues, Physics in medicine and biology 41 (1996) 2271. http://dx.doi.org/10.1088/0031-9155/41/11/003

[7] A. V. Vorst, A. Rosen, Y. Kotsuka, RF/microwave interaction with biological tissues, Wiley series in microwave and optical engineering, Hoboken, N.J. : John Wiley & Sons : IEEE, c2006., 2006.

[8] A.Poon, S. O'Driscoll, T. Meng, Optimal frequency for wireless power transmission into dispersive tissue, IEEE Trans. Antennas Propag. 58 (5) (2010) 1739–1750. http://dx.doi.org/10.1109/TAP.2010.2044310

[9] C. A. Balanis, Antenna Theory: Analysis and Design, 3rd Edition, John Wiley and Sons, Inc., 2005.

[10] R. Bashirullah, Wireless Implants, IEEE Microw. Mag. 11 (7) (2010) 14–23. http://dx.doi.org/10.1109/MMM.2010.938579

[11] M. Zargham, P. Gulak, Maximum achievable efficiency in near-field coupled power-transfer systems, IEEE Trans. Biomed. Circuits Syst. 6 (3) (2012) 228–245. http://dx.doi.org/10.1109/TBCAS.2011.2174794

[12] J. Do, D. Akos, P. Enge, L and S bands Spectrum Survey in the San Francisco Bay Area, in: Position Location and Navigation Symposium (PLANS), 2004, pp. 566–572.

[13] S. Nagaraj, S. Khan, C. Schlegel, M. Burnashev, Differential preamble detection in packet-based wireless networks, IEEE Trans. Wireless Commun. 8 (2) (2009) 599–607. http://dx.doi.org/10.1109/TWC.2009.071169

[14] Rezaei, Navid, et al. "Electromagnetic Energy and Data Transfer in Biological Tissues Using Loop Antennas." *Procedia Computer Science* 19 (2013): 908-913. http://dx.doi.org/10.1016/j.procs.2013.06.124

[15] M. Ahmadi, B. Cockburn, and C. Schlegel, "Low power asynchronous packet- based baseband transceiver for wireless sensor networks," in Proc. IEEE Int. Midwest Symp. on Circuits and Systems (MWSCAS), Aug. 2012, pp. 940–943.

[16] D. Bol, R. Ambroise, D. Flandre, and J.-D. Legat, "Interests and Limitations of Technology Scaling for Subthreshold Logic," IEEE Trans. VLSI Syst., vol. 17, no. 10, pp. 1508–1519, 2009. http://dx.doi.org/10.1109/TVLSI.2008.2005413

[17] D. Bol, "Pushing ultra-low-power digital circuits into the nanometer era," Ph.D. dissertation, Universit`e Catholique de Louvain, December 2008.

[18] N. Rezaei S., "Electromagnetic Energy and Data Transfer for Low-Power Implantable Biomedical Devices," M.Sc. dissertation, University of Alberta, Fall 2013.

Appendix A

The received signal power is the transmit power that remains after overcoming path losses and antenna directional gains, and is given by

$$P_R = P_T + P_L \quad [\text{dBm}] \qquad \text{(A.1)}$$

where P_L is the total path loss in dB, including the tissues, free path loss and the antenna gains, and P_T is the transmit power in dBm.

The noise power in the receiver can be expressed as in Eq. A.2. The noise power spectral density in the 2.4-GHz ISM band is calculated as explained in Sec. 3.1.

$$P_N = \text{PSD}_\text{n} + 10\log(W_n) + \text{NF} \quad [\text{dBm}] \qquad \text{(A.2)}$$

where PSD_n is the noise spectral density in the 2.4-GHz ISM band, and NF is the receiver noise figure in dB, which is due to noise enhancement by the receiver's own circuitry. In our case, the PSD_n is equal to thermal noise and is calculated as $10\log(kT_0 \cdot 10^3)$ in dBm/Hz unit, where k is the Boltzman constant and T_0 is the ambient temperature.

Recall that the SNR in dB is the difference of the received signal power and noise ($\mathrm{SNR} = P_R - P_N$). Using this equation and then Eqs. 5, A.1 and A.2, the required transmit power to achieve a certain quality of reception is given by

$$P_T = 10\log\left(R_c \cdot \frac{E_c}{N_0} \right) + 10\log(kT_0 \cdot 10^3) + \mathrm{NF\text{-}P_L} \quad [\mathrm{dBm}] \text{ (A.3)}$$

The energy required to transmit one chip from the transmitter antenna to the receiver antenna, E_{ct} , is given by

$$E_{ct} = \frac{P_T - P_R}{R_c} \quad [\mathrm{J/chip}] \text{ (A.4)}$$

where R_c is in Hz, P_T and P_R are in W, and E_{ct} is in J/chip.

Using Eq. A.1, received power is calculated as

$$P_R = P_T \cdot 10^{(P_L/10)} \quad [\mathrm{W}] \text{ (A.5)}$$

Using Eq. A.3, the value of the transmitted power in watts (W) can be calculated as

$$P_T = (kT_0 \cdot R_c \cdot \frac{E_c}{N_0}) \cdot 10^{((NF - P_L)/10)} \quad [\mathrm{W}] \text{ (A.6)}$$

By substituting Eq. A.6 into Eq. A.5 and substituting Eqs. A.5 and A.6 into Eq. A.4, the energy to transmit one chip is calculated as follows

$$E_{ct} = kT_0 \cdot \frac{E_c}{N_0} \cdot 10^{((NF - P_L)/10)} \cdot \left(1 - 10^{(P_L/10)}\right) \quad [\mathrm{J/chip}] \text{ (A.7)}$$

The energy to transmit one bit is then $E_{bt} = E_{ct} \cdot L_b$, where L_b is the spread-spectrum processing gain.